

SPATIOTEMPORAL STRUCTURE IN INTENSE THz PULSED BEAMS

G. A. Hine*, Oak Ridge National Laboratory, Oak Ridge, TN, USA

Abstract

Optically generated terahertz radiation, with gigavolt per meter (GV/m) electric fields accessible in tabletop experiments, provides a promising source of accelerating gradients for future particle accelerator applications. Manipulation and characterization of radiation is essential for efficiently producing high fields and effectively delivering them to an accelerating structure or interaction region. A method of generating and characterizing high quality and structured terahertz pulsed laser beams for compact particle acceleration is presented.

INTRODUCTION

Electromagnetic radiation with linear frequency in the 0.3-300 terahertz (1THz = 10^{12} Hz) band is referred to as Terahertz, THz, or T-Wave radiation. It comprises millimeter and sub-millimeter spatial scales and few picosecond to subpicosecond time scales. The production of coherent THz radiation has been demonstrated by a wide range of mechanisms from vacuum electronics to nonlinear optics using intense lasers. Although achieving high radiative power in this band has been historically difficult, this is an active field of research in which significant improvements are rapidly being demonstrated [1–3].

Because of its short length- and time-scales compared to microwaves, tightly focused THz pulses with high temporal (sub-picosecond) compression are possible, yielding extremely high electric fields even with modest pulse energy [4]. This has enabled a breadth of research from advanced particle acceleration and manipulation schemes [5–7] to fundamental physics and materials science [8–10]. At Spallation Neutron source, we are investigating using high THz fields to emulate the conditions inside a

superconducting cavity to improve cavity processing and mitigate deleterious effects like field emission [11] and as a possible source of accelerating gradients for novel ion acceleration schemes.

One method of THz generation (Fig. 1), optical rectification in nonlinear ($\chi^{(2)}$) materials has been shown to produce pulses with high fields (> 10 V/m) in free-space (no resonant structure) at comparatively high conversion efficiencies (2%) [4]. In these materials, a local quasi-static polarization develops in proportion to the time-averaged intensity of the pump laser pulse. As each unit cell in the crystal polarizes and depolarizes, it radiates a pulse with a single electromagnetic cycle. The radiation from each cell superposes like a phased antenna array, producing a directed pulse of THz radiation with a transverse profile determined by the pump transverse properties. With a conventional nonlinear optics treatment (one temporal dimension + one longitudinal

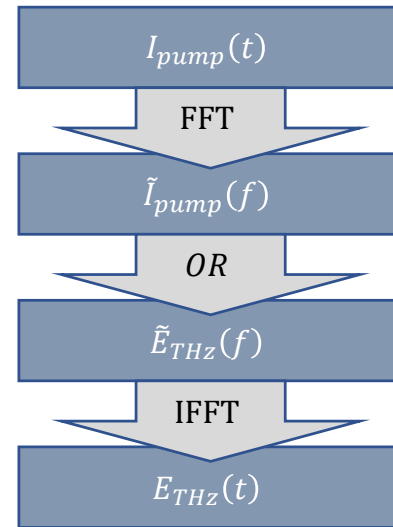


Figure 1: Calculation of THz pulses by optical rectification. The 1350 nm pump temporal profile is estimated from measurements of the 800 nm pulse input into the OPA. The power spectrum of the pump is calculated by FFT of the estimated pump profile. The THz amplitude spectrum generated in a $\chi^{(2)}$ medium like OH1 is proportional to the pump spectrum with a frequency-dependent prefactor Eq. (1). The THz temporal profile is Then calculated by IFFT of the generated THz amplituded spectrum.

dimension) as in [12], the generated THz pulse can be described by Eq. (1). Since the crystal itself is uniform, a pump which overfills a circular aperture should produce a THz pulse with a flat-top profile with a uniform spectrum throughout,

$$\begin{aligned} \tilde{A}_0 &= B(f)L(f, z)\tilde{I}_{pump}(f) \\ B(f) &= \frac{2d_{THz}f^2}{n_0\epsilon_0c^3\left(\frac{2\pi f}{c}(n_{THz}(f) + n_g) + i\left(\frac{\alpha_{THz}(f)}{2} + \alpha_0\right)\right)} \\ L(f, z) &= \frac{e^{i\left(\frac{2\pi f}{c}n_{THz} + i\alpha_{THz}/2\right)z} - e^{i\left(\frac{2\pi f}{c}n_g + i\alpha_0\right)z}}{\left(\frac{2\pi f}{c}(n_{THz}(f) - n_g) + i\left(\frac{\alpha_{THz}(f)}{2} - \alpha_0\right)\right)} \end{aligned} \quad (1)$$

The variables in Eq. (1) are described and their values defined in Table 1. Since the refractive index and absorption coefficient varies significantly over the generated THz range of interest, the refractive index $n_{THz}(f)$ and absorption coefficient $\alpha_{THz}(f)$ are expressed as functions of frequency according to the a lorentz multiple oscillator model described in [13].

The resulting THz spectrum is extremely broadband in the sense that its frequency spread is on the order of the peak or center frequency. While effects like “chirping” due to material dispersion are important for pulses with a few percent

* hinega@ornl.gov

Table 1: Values used for calculating THz electric fields generated in OH1 using a 1350 nm pump. Material properties for OH1 were obtained from [3].

Parameter	Value	Description
d_{THz}	280 pm/V	nonlinear coefficient for THz generation
n_g	2.33	group refractive index at pump center frequency
n_0	2.16	refractive index at pump center frequency
α_0	0.100 1/mm	absorption coefficient at pump center frequency
z	0.56 1/mm	OH1 thickness
ϵ_0	8.854 F/m	vacuum permittivity
c	0.300 mm/ps	speed of light in vacuum

bandwidth, for subcycle THz pulses, where the spectrum can span multiple octaves, even propagation in free space can challenge intuition. In [14] spectral changes were observed in the propagation of such a broadband THz pulse through its focus. Since the spectral content of a pulse should not change under linear propagation, this effect was attributed to a transverse redistribution of the frequency content throughout the focus.

In [15], the transverse redistribution of frequencies in sub-cycle THz pulses was directly observed using a method for obtaining the 2-transverse + 1-temporal dimensional (2+1D) spatio-temporal profile of the pulse. Pulses with these bandwidths which are initially spatio-spectrally uncorelated exhibit a spatiotemporal structure which is pinched at its center, resembling a piece of farfalle pasta, when focused. Subsequently, transmission through an uneven medium was shown to produce spatio-temporal optical vortices, robust defects embedded in the spatio-temporal phase of the pulse [16]. At such broad bandwidths, spatio-temporal effects become increasingly important and even the most fundamental elements of linear propagation are complicated.

The method for observing the spatio-temporal profile of the pulse is based on conventional electro-optic sampling (see [17, 18]), which utilizes the Pockels effect, where a $\chi^{(2)}$ material exhibits a birefringence in proportion to a static or quasi-static applied electric field. An ultrashort (less than the THz pulse period) probe co-propagating with a THz pulse in this medium will undergo a polarization rotation according to the instantaneous THz field strength. By scanning the delay between THz and probe pulses, a THz temporal electric field profile can be ascertained. Since this effect is also local in space, a probe which is transversely larger than the THz pulse will imprint the transverse profile of the THz electric field at each delay. Stacking a series of these transverse profiles over a range of THz-probe delay, a spatio-temporal profile of the pulse is constructed which retains spatio-temporal correlations. The 2-transverse + 1-temporal measurement is a particularly useful characterization of a linearly polarized terahertz pulse because it provides suffi-

cient information to calculate the subsequent evolution of the pulse according to the Huygens principle.

METHODS

Observing these spatio-temporal effects requires a measurement that retains spatio-temporal correlations. This is not true for widely used microbolometer focal plane arrays, which measure fluence as a function of transverse coordinate, integrating intensity over the temporal dimension. Nor is it true for conventional electro-optic sampling (EOS) using a balanced photodetector, which only captures the electric field around a point in the transverse profile, typically where the largest peak field is located. Recently, a coherent spatio-temporal technique has been demonstrated which captures the full spatio-temporal (and thus spatio-spectral) profile of the THz pulse [15, 19]. Such a measurement which captures both wavefront curvature and temporal (or spectral) phase over the whole 2-transverse + 1-temporal dimensional profile of coherent radiation is extremely rare in optics and provides a clearer picture of the whole pulse compared to what might be constructed from separate uncorrelated measurements.

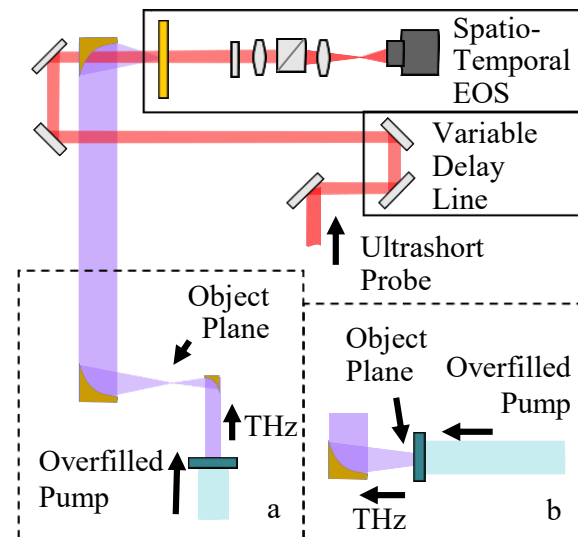


Figure 2: Experimental Setup. An 800 nm ultrashort probe (red) passes through a variable delay line and overlaps with the THz in a GaP crystal (orange). The probe undergoes a polarization rotation proportional to the local instantaneous THz electric field strength, and is relayed through a polarization selecting imaging system to a CCD. The collection of images at various delays, along with a reference in the absence of the THz, constitutes the spatio-temporal electro-optic sampling method, and is described in detail in [15, 19]. The THz source was used in two configurations, both with the 1350 nm pump overfilling the OH1 clear aperture. In configuration (a) the THz is focused by a 1/2" off-axis parabola with RFL = 1", and the focus relayed to the spatio-temporal EOS setup. In configuration (b), the OH1 is at the object plane of the two-OAP imaging system and is directly imaged to the spatio-temporal EOS.

Using the method described in [15], the spatio-temporal profile of THz pulses were measured at at the exit of the crystal and at the pulse focus. The experimental setup is depicted in Fig. 2. Because of space constraints, the pulse is relayed with an imaging system consisting of two gold coated off-axis parabolic mirrors (OAPs). An ultrashort probe with variable delay is focused through a drilled hole in the last mirror and overlaps the THz pulse in an electro-optic crystal. The THz field, by inducing a quasi-static birefringence in the electro-optic medium, causes a small polarization transformation proportional to its electric field strength. The initially vertically polarized probe is imaged at the exit of the electro-optic crystal to a ccd through a quarter wave plate and polarizer, selecting a circular polarization state. In this configuration, small changes in the probe intensity are proportional to the instantaneous THz electric field [19],

$$E_{\text{THz}} \propto (V(E_{\text{THz}})/V_0 - 1) \quad (2)$$

where $V(E_{\text{THz}})$ is the level on the ccd in the presence of the THz field, and V_0 is the level in the absence of THz. Spatiotemporal scans were performed averaging "8"-frames at each time and acquiring background images intercolated with signal. The assembly of electro-optic medium and polarization-selecting imaging system are referred to here as spatio-temporal EOS. Initially, the THz source was placed at the object plane of the two-OAP imaging system Fig. 2 b, and the THz at the source relayed directly to the spatio-temporal EOS assembly. Subsequently, the THz source was moved upstream and an additional parabolic mirror was introduced with the focus at the object plane (Fig. 2 a).

THz pulses were generated in OH1 as in [15]. It was illuminated with the 300 μJ 1350 nm output of an optical parametric amplifier (OPA), pumped with 4 mJ, 800 nm 35 fs pulses. The pump profile overfilled the aperture of the OH1 crystal (6 mm). The uniform illumination produces a flat-top transverse profile and uncorrelated spectrum, and the low absorptive losses of the OH1 produce a sine-like sub-cycle pulse. In the first configuration (Fig. 2 b), the exit face of the OH1 is relayed by two off-axis parabolic mirrors with 3 \times demagnification directly to the spatio-temporal electro-optic sampling assembly. In the second configuration (Fig. 2 a), the output of the OH1 was focused with a 1/2", RFL = 1" off-axis parabolic mirror and the OH1 moved just ahead of it. The ultrashort probe was picked off from the 800 nm pump for the OPA, and the electro-optic medium used was GaP.

RESULTS

The pump is nearly uniform over the OH1 clear aperture, resulting in a nearly identical THz spectrum generated everywhere throughout the crystal. This generates a flat-top THz pulse with sine-like carrier envelope phase that has little spatio-spectral or spatio-temporal correlation. Therefore, the transverse and temporal (or spectral) parts of the pulse can be separated into independent functions, and the THz

electric field can be described by,

$$E_{\text{THz}}(r, t) = \begin{cases} 2\Re \left(\int_0^\infty df i e^{i2\pi ft} \tilde{A}_0(f) \right), & \text{for } r < R_0 \\ 0, & \text{otherwise} \end{cases} \quad (3)$$

where $\tilde{A}_0(f)$ is the THz spectrum generated according to the pump temporal properties (Eq. (1)), and R_0 is the radius of the clear aperture of the crystal. The resulting spectrum and pulse are calculated and compared with on-axis measurements at the OH1 crystal (Fig. 2 b) in Figs. 3 a and c with good agreement. The measured spectrum is calculated by FFT of the measured pulse and the theoretical pulse calculated by IFFT of the theoretical spectrum. An x-t slice of the full spatio-temporal pulse measurement in this configuration is shown in Fig. 3 e which has a flat-top profile due to the uniform illumination of the pump across the crystal clear aperture. The corresponding amplitude spatio-spectrum in Fig. 3 f is calculated by FFT in the temporal direction, and is mostly uncorrelated.

Once the uncorrelated flat-top pulsed beam is focused, as in Fig. 2 a, the spatio-spectrum can no longer be considered uncorrelated [15] and thus the spatial and temporal parts cannot be separated. At the focus, each flat-top profiled frequency component focuses to an Airy disk with transverse size inversely proportional to frequency,

$$E_{\text{THz}}(r, t) = 2\Re \left(\int_0^\infty df -i e^{i2\pi ft} D_{\text{NA}} \frac{2J_1(4\pi \text{NA} fr/c)}{4\pi \text{NA} fr/c} \frac{2\pi f}{c} \tilde{A}_0(f) \right) \quad (4)$$

where NA is the numerical aperture of the focus, and D_{NA} is an overall scale factor following from the numerical aperture.

A spatio-spectrum assembled from these Airy disks is shown in Fig. 3 j. The spatio-temporal form of the pulsed beam was calculated and is shown in Fig. 3 i, and resembles the "farfalle" pulse as calculated by a superposition of gaussian beams as in [15], although the wavefronts in the periphery of the Airy-disk farfalle appear straighter and extend further than those of the gaussian equivalent. Similarly, the Airy-disk type spatio-spectrum resembles the gaussian spatio-spectrum in [15], but having curved fringes in its wings. Since the propagation of this pulsed beam is not self-similar, a proper Guoy phase term cannot be separated from the pulse evolution. Nonetheless, because each frequency is advanced by $\pi/2$ at the focus, the initially sine-like carrier envelope phase also advances by $\pi/2$ producing a cosine-like shape. This was accounted for by applying a phase prefactor of $-i$ in Eq. (4).

The x-t slices of the spatio-temporal measurement and spatio-spectrum for the focusing configuration (Fig. 2 a) is shown in Fig. 3 g and h respectively. The spatio-temporal structure of the focused pulsed shows flaring of the wavefronts in the fore and aft of the pulse and the spatio-spectrum has a horn shape, characteristic of a focused ultrabroadband pulsed beams [15], in good qualitative agreement with the Airy-disk model. The pulse and spectrum on the central axis of the measurement is compared with those of the model

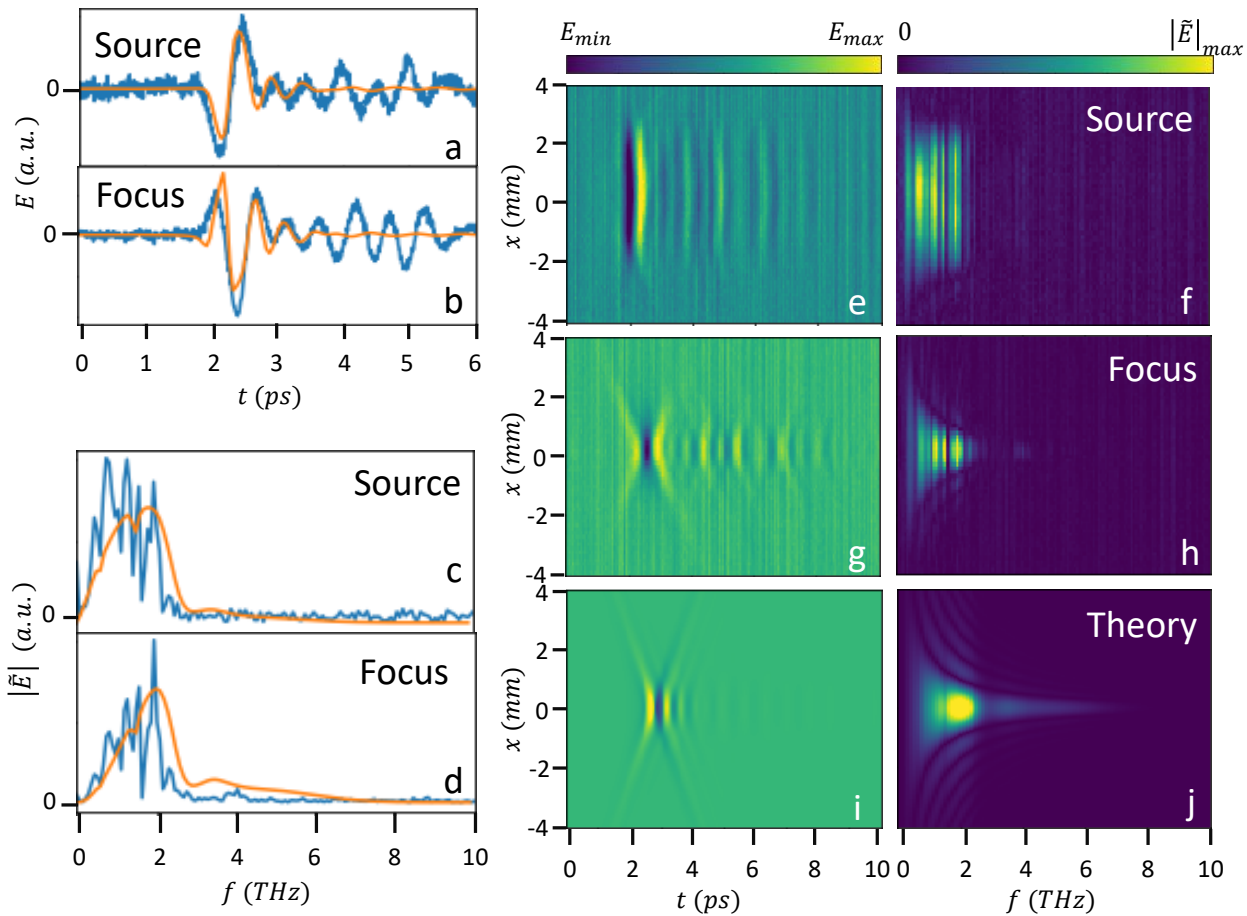


Figure 3: Data compared to theory. (a) The pulse calculated using Eq. (1) with material parameters from Table 1 at the exit of the OH1 crystal in orange overlaid on measurement in blue, showing good agreement for the main pulse. (b) The temporal evolution on-axis for a focused pulse, accounting for the spatio-temporal distribution of spectral content according to Eq. (4). Trailing oscillations in data and slight variations in the temporal phase of the main pulse are attributed to propagation through air with ambient humidity and multiple reflections of the in the GaP. (c,d) Magnitude of amplitude spectra corresponding to (a) and (b) respectively. Measured spectra in blue show good agreement with theory in orange, with modulations in blue attributed to multiple reflections in the GaP and scattering in ambient humidity. Current limitations on probe pulse length are limiting measurement bandwidth above about 3 THz. Both measured and calculated spectra at the focus are seen to be visibly bluer than at the source, with the calculated spectrum exhibiting a high-frequency tail which is much less prominent in the overall spectrum seen at the source. (e,g) Measured Spatio-temporal profiles of THz pulses generated in OH1, imaged from the source and focus respectively. (e) appears flat-topped due to a pump which overfills the clear aperture of the OH1 mount, while (g) exhibits the farfallé-shape characteristic of focused ultrabroadband pulses [15]. (f) and (h) show the magnitude of spatio-spectral amplitude corresponding to (e) and (g) respectively. The spatio-spectrum at the source is mostly uncorrelated, as expected near the source, while the focused pulse is highly correlated, showing the characteristic horn-shape as well as side bands corresponding to higher order maxima of the constituent monochromatic Airy disks. (i,j) Spatio-temporal profile and spatio-spectrum calculated according to Eq. (4) showing prominent x-shaped wings in the spatio-temporal domain and a banded horn in the spatio-spectral domain. The tail of the spatio-spectrum is prominent, although it only makes up a small fraction of the overall spectrum.

in Figs. 3 b and d respectively, with similar phase and spectral characteristics.

Some effects which are not included in this model which could explain discrepancies between the measured and theoretical pulsed beams and spatio-spectra. The measured pulsed beams have trailing oscillations and the carrier envelope phase of the focused beam is slightly different from that of the model. This can be attributed to propagation

through air with ambient humidity, causing an accumulation of group-delay dispersion and scattering at certain frequencies. There are also multiple reflections in the GaP, which altogether cause the measured spectra in Figs. 3 a–d to be somewhat modulated.

The measured spectra are also narrower and redder than predicted by the model, which is attributed to limitations in the bandwidth of the measurement. Although electro-optic

Content from this work may be used under the terms of the CC BY 4.0 licence (© 2021). Any distribution of this work must maintain attribution to the author(s), title of the work, publisher, and DOI

sampling in GaP has been demonstrated with bandwidth beyond 7 THz, the probe pulse length in this experiment limited bandwidth to about 3 THz. The model and measured spectra show good agreement in the 0-2 THz range, particularly in the difference between focused and unfocused spectra. The unfocused spectrum appears to be linear in the vicinity of 0, while the focused spectrum could be called quadratic. This is consistent with the redistribution of frequencies that occurs when an initially uncorrelated pulsed beam is focused with a common numerical aperture [15] and is included in Eq. (4) with a factor proportional to $\sin^2(\theta)$ and is included in Eq. (4) with a factor proportional to $\sin^2(\theta)$.

Although the measured data shows blue-shifting of the source spectrum upon focusing, this effect is more pronounced in the model, which is not limited by the measurement bandwidth. The model shows the development of a long high-frequency tail at the focus which is hardly present in the source spectrum. This, along with the diminished low-frequency content can result in mischaracterization of the overall pulsed beam, with mean frequency on-axis at the focus twice that of the overall frequency content of the pulse.

CONCLUSION

A model of THz pulse generation by optical rectification in OH1 shows good agreement with spatio-temporal measurements over the bandwidth of the measurement.

THz pulses at the exit of an OH1 crystal with uniform illumination are uncorrelated, having similar spectra throughout the transverse profile. The uncorrelated pulse generated in the OH1 is sine-like and becomes a highly correlated cosine-like pulse at the focus.

The focused THz spectrum exhibits a horn-like shape, with curved fringes which is well described by a superposition of Airy disks of different frequencies, focused with a common numerical aperture. The spectra on-axis in the focused pulse is significantly bluer than the spectra at the source and the overall spectral content at the pulse, and therefore the application of ultrabroadband THz pulses must be treated with a deference to their spatio-temporal characteristics.

REFERENCES

- [1] J. H. Booske *et al.*, “Vacuum Electronic High Power Terahertz Sources”, *IEEE Trans. Terahertz Sci. Technol.*, vol. 1, no. 1, pp. 54-75, Sept. 2011. doi:10.1109/TTHZ.2011.2151610
- [2] J. Hebling, K. Yeh, M. C. Hoffmann, and K. A. Nelson “High-Power THz Generation, THz Nonlinear Optics, and THz Nonlinear Spectroscopy”, *IEEE J. Sel. Top. Quantum Electron.*, vol. 14, no. 2, pp. 345-353, 2008. doi:10.1109/JSTQE.2007.914602
- [3] M. Jazbinsek, U. Puc, A. Abina, and A. Zidanzek, “Organic Crystals for THz Photonics”, *Appl. Sci.*, vol. 9, p. 882, 2019. doi:10.3390/app9050882
- [4] M. Shalaby and C. Hauri, “Demonstration of a low-frequency three-dimensional terahertz bullet with extreme brightness”, *Nat. Commun.*, vol. 6, p. 5976, 2015. doi:10.1038/ncomms6976
- [5] M. T. Hibberd *et al.*, “Acceleration of relativistic beams using laser-generated terahertz pulses”, *Nat. Photonics.*, vol. 14, pp. 755-759, 2020. doi:10.1038/s41566-020-0674-1
- [6] E. Nanni *et al.*, “Terahertz-driven linear electron acceleration”, *Nat. Commun.*, vol. 6, p. 8486, 2015. doi:10.1038/ncomms9486
- [7] D. Zhang *et al.*, “Femtosecond phase control in high-field terahertz-driven ultrafast electron sources”, *Optica*, vol. 6, pp. 872-877, 2019. doi:10.1364/OPTICA.6.000872
- [8] Ryusuke Matsunaga, Yuki I. Hamada, Kazumasa Makise, Yoshinori Uzawa, Hirota Terai, Zhen Wang, and Ryo Shimano, “Higgs Amplitude Mode in the BCS Superconductors Nb_{1-x}Ti_xN Induced by Terahertz Pulse Excitation”, *Phys. Rev. Lett.*, vol. 111, p. 057002, 2013. doi:10.1103/PhysRevLett.111.057002
- [9] Sachiko Nakamura, Yudai Iida, Yuta Murotani, Ryusuke Matsunaga, Hirota Terai, and Ryo Shimano, “Infrared Activation of the Higgs Mode by Supercurrent Injection in Superconducting NbN”, *Phys. Rev. Lett.*, vol. 122, p. 257001, 2019. doi:10.1103/PhysRevLett.122.257001
- [10] I. C. Benea-Chelmus *et al.*, “Electric field correlation measurements on the electromagnetic vacuum state”, *Nature*, vol. 568, pp. 202-206, 2019. doi:10.1038/s41586-019-1083-9
- [11] Marc Doleans, “Ignition and monitoring technique for plasma processing of multicell superconducting radio-frequency cavities”, *J. Appl. Phys.*, vol. 120, p. 243301, 2016. doi:10.1063/1.4972838
- [12] A. Schneider *et al.*, “Generation of terahertz pulses through optical rectification in organic DAST crystals: theory and experiment”, *J. Opt. Soc. Am. B: Opt. Phys.*, vol. 23, pp. 1822-1835, 2006. doi:10.1364/JOSAB.23.001822
- [13] F. D. J. Brunner *et al.*, “A hydrogen-bonded organic nonlinear optical crystal for high-efficiency terahertz generation and detection”, *Opt. Express*, vol. 16, pp. 16496-16508, 2008. doi:10.1364/OE.16.016496
- [14] C. Ruchert, C. Vicario, and C. P. Hauri, “Spatiotemporal Focusing Dynamics of Intense Supercontinuum THz Pulses”, *Phys. Rev. Lett.*, vol. 110, p. 123902, 2013. doi:10.1103/PhysRevLett.110.123902
- [15] G. A. Hine and M. Doleans, “Intrinsic spatial chirp of subcycle terahertz pulsed beams”, *Phys. Rev. A*, vol. 104, p. 032229, 2021. doi:10.1103/PhysRevA.104.032229
- [16] G. Hine, “Observation of Spatiotemporal Optical Vortices in Subcycle Terahertz Pulses”, *Front. Opt. + Laser Sci.*, 2021. doi:10.1364/FIO.2021.JTu7A.5
- [17] Q. Wu and X. C. Zhang, “7 terahertz broadband GaP electro-optic sensor”, *Appl. Phys. Lett.*, vol. 70, p. 1784, 1997. doi:10.1063/1.118691
- [18] S. Casalbuoni, H. Schlarb, B. Schmidt, P. Schmüser, B. Steffen, and A. Winter, “Numerical studies on the electro-optic detection of femtosecond electron bunches”, *Phys. Rev. ST Accel. Beams*, vol. 11, p. 072802, 2008. doi:10.1103/PhysRevSTAB.11.072802
- [19] G. A. Hine, “Spatio-Temporal Measurements of THz Pulses”, in *Proc. IPAC'21*, Campinas, Brazil, May 2021, pp. 4021-4023. doi:10.18429/JACoW-IPAC2021-THPAB131